

Cross-CBAM: A Lightweight network for Scene Segmentation

Zhengbin Zhang^a, Zhenhao Xu^a, Xingsheng Gu^a and Juan Xiong^b

^aEast China University Of Science And Technology, No.130, MeiLong Road, XuHui District, Shanghai, 200237, China

^bUniversity of Shanghai for Science and Technology, No.516, JunGon Road, YangPu District, Shanghai, 200093, China

ARTICLE INFO

Keywords:

Real-time semantic segmentation
Scene Segmentation
Deep learning
Attention mechanism

ABSTRACT

Scene parsing is a great challenge for real-time semantic segmentation. Although traditional semantic segmentation networks have made remarkable leap-forwards in semantic accuracy, the performance of inference speed is unsatisfactory. Meanwhile, this progress is achieved with fairly large networks and powerful computational resources. However, it is difficult to run extremely large models on edge computing devices with limited computing power, which poses a huge challenge to the real-time semantic segmentation tasks. In this paper, we present the Cross-CBAM network, a novel lightweight network for real-time semantic segmentation. Specifically, a Squeeze-and-Excitation Atrous Spatial Pyramid Pooling Module(SE-ASPP) is proposed to get variable field-of-view and multiscale information. And we propose a Cross Convolutional Block Attention Module(CCBAM), in which a cross-multiply operation is employed in the CCBAM module to make high-level semantic information guide low-level detail information. Different from previous work, these works use attention to focus on the desired information in the backbone. CCBAM uses cross-attention for feature fusion in the FPN structure. Extensive experiments on the Cityscapes dataset and Camvid dataset demonstrate the effectiveness of the proposed Cross-CBAM model by achieving a promising trade-off between segmentation accuracy and inference speed. On the Cityscapes test set, we achieve 73.4% mIoU with a speed of 240.9FPS and 77.2% mIoU with a speed of 88.6FPS on NVIDIA GTX 1080Ti.

1. Introduction

Semantic segmentation is one of the main tasks of computer vision, where the goal is to classify all pixels in an image with a dense label classification. Advances in deep learning have greatly boosted the accuracy of semantic segmentation in several benchmarks, e.g., Pascal Voc[9], ADE 20k[45], Microsoft COCO[24], and Cityscapes[7]. Due to its excellent performance, it has been widely used in autonomous driving, medical image segmentation, machine vision and other fields. However, these applications place higher requirements for mobile deployment.

To meet the demands of these fields, a lot of researchers have proposed real-time semantic segmentation models with low parameter quantity and high inference speed. These models reduce inference time from two perspectives: 1) try to restrict the input image size [35], or prune redundant channels in the networks [1][28][42] to reduce computation complexity and boost the inference speed. Fewer channels and smaller input resolution of an image seem to be effective (or work), however, it can easily lose spatial details around boundaries, corners, and small objects, leading to the loss of metric accuracy. 2) try to choose lightweight backbones [5, 14] to reduce parameters and Flops. Most of these lightweight networks take advantage of the ImageNet1k pre-trained weights for faster training and higher accuracy. But, this approach poses two serious problems. First, ImageNet1k has one thousand classes, to classify each image, the backbone used to train ImageNet1k typically contains thousands of channels in the last few convolutional layers, resulting in redundant channels. The second point is that the input size of ImageNet1k is smaller than the

segmentation, resulting in the lack of sufficient receptive field and detail information in the ImageNet1k network.

To tackle the above problems, BiSeNet[39] and BiSeNetV2 [38] propose a multi-path structure to extract low-level details and high-level semantics. U-Net[30] adopts the U-shape framework to gradually reduce channels and increase spatial resolution. Therefore, it can compensate some spatial details lost due to downsampling. DDRNet[13] proposes a dual-resolution network with two parallel depth branches with different resolution. But adding another path increases model complexity and inference time. At the same time, the auxiliary path always lacks low-level information guidance.

In this paper, we propose a novel hand-craft network with the aim of improving higher segmentation accuracy, explainable structure, and competitive performance to that of existing methods. The network is named Cross-CBAM. As illustrated in Figure 1, the Cross-CBAM network adopts the encode-decode architecture and consists of two novel modules: Squeeze-and-excitation Atrous Spatial Pyramid Pooling Module(SE-ASPP) and Cross Convolutional Block Attention Module(CCBAM). The motive and design details of the above modules are presented below.

In detail, to overcome the large number of parameters and slow inference speed caused by the multi-path encoder, we employ Short-Term Dense Concatenate network-STDC[10] derived from DenseNet[19] as our backbone. In order to obtain variable receptive fields with fewer parameters, the number of filters of convolutional layers in the STDC blocks is gradually reduced. The STDC module concatenates response maps from multiple consecutive layers, each encoding input images/features at different scales and respective domains, resulting in a multi-scale feature representation. Enhanced feature representation plays a crucial role in improving semantic segmentation accuracy[21, 32].

✉ y80210135@main.ecust.edu.cn (Zhengbin Zhang)
ORCID(s): 0000-0002-4747-1147 (Zhengbin Zhang)

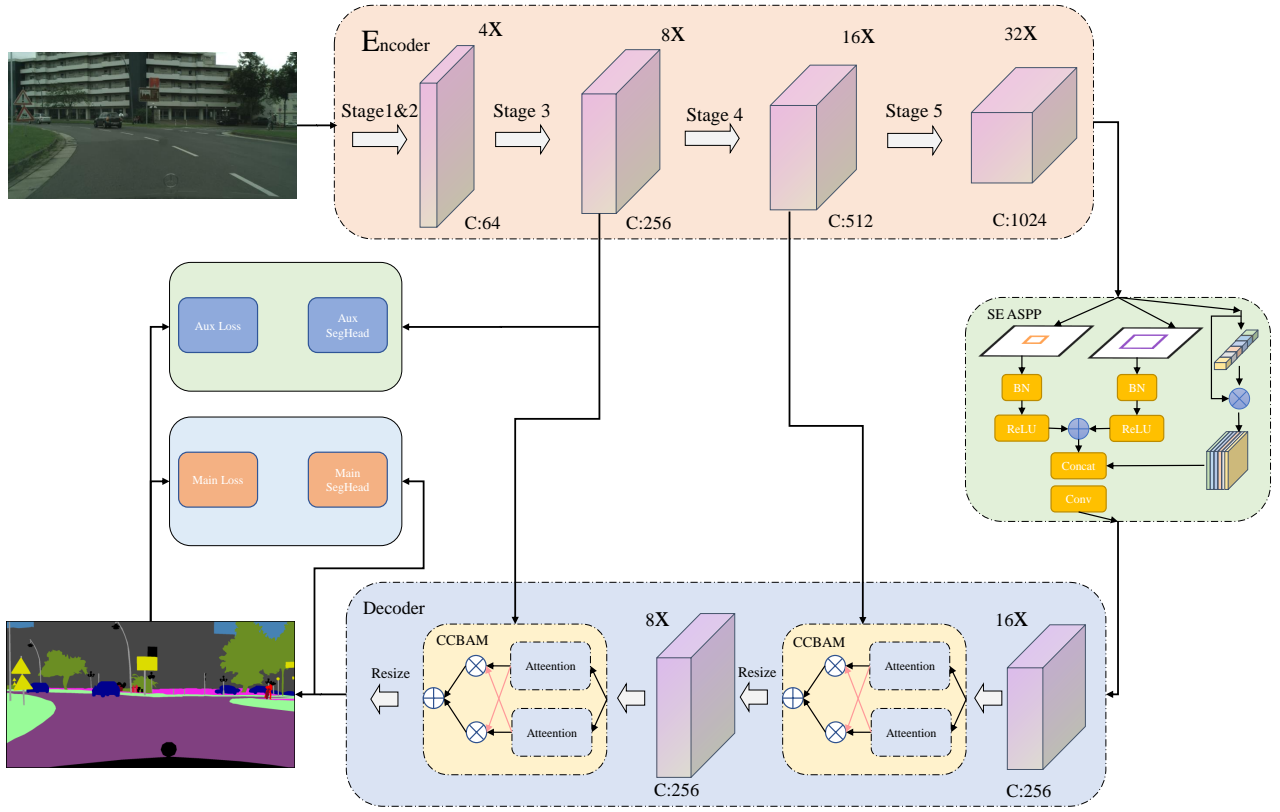


Figure 1: Overview of the proposed architecture. *Encoder* denotes the STDC network, which consists of five stages, *Decoder* denotes the proposed method, *CCBAM* and *SE-ASPP* denote the innovative structures, respectively. *Conv* & *BN* are used for channel transformation, and *Resize* means bilinear interpolation upsampling. *C* represents the number of channels, and *4X* refers to the multiple of downsampling the original image.

It is usually achieved by fusing the output features from the low-level and high-level of the decoder. However, the existing fusion models are too complex, resulting in a huge amount of model parameters. In this work, we propose a Cross Convolutional Block Attention Module (CCBAM) to strengthen feature representations efficiently. As shown in Figure 3, CCBAM first utilizes a cross-attention module for fusing features. It uses both channel attention and spatial attention, channel attention emphasizes 'what' while spatial attention emphasizes 'where'.

Variable receptive fields and multi-scale information are key factors to improve semantic segmentation accuracy. Existing methods such as parallel Atrous Spatial Pyramid Pooling module (ASPP)[3] adopt four parallel atrous convolutions to obtain multi-scales. It expands the receptive fields while increasing parameters, which is time-consuming for real-time networks. Therefore, we design an innovative and lightweight module called the Squeeze-and-Excitation Atrous Spatial Pyramid Pooling Module (SE-ASPP) to expand the field of view of filter. SE-ASPP only keeps two parallel atrous convolutions, and replaces the concatenate

operation with an add operation. We replace image pooling in ASPP with a SE attention module.

Our main contributions can be summarized as follows:

- A new feature fusion module called CCBAM is designed. It boasts the cross-multiplication operation that enables high-level semantic information to guide low-level details information. And it leverages channel and spatial attention to strengthen the feature representations.
- A Squeeze-and-Excitation Atrous Spatial Pyramid Pooling Module (SE-ASPP) is proposed, which can not only obtain a larger and variable receptive field, but also multiple scales. While SE-ASPP reduces the complexity of the model and ensures the accuracy of the segmentation.
- A lightweight attention segmentation network is designed for the real-time semantic segmentation task network. Cross-CBAM utilizes contextual attention fusion module (CCBAM) to fuse information, and utilizes SE-ASPP to further improve the accuracy at a very small cost of speed.

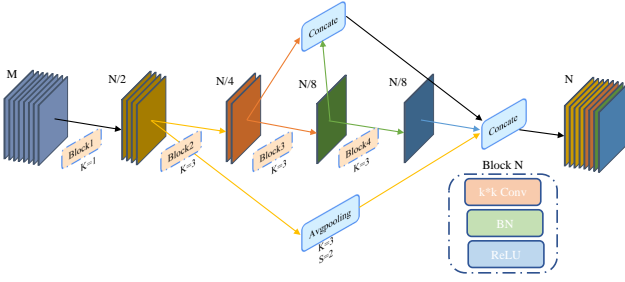


Figure 2: The STDC module used in our network. *Block i* operation includes Conv-BN-ReLU, *Avgpooling* operation refers to average pooling with stride=2 and kernel-size=3. *M* denotes the dimension of the input channels, and *N* denotes the dimension of the output channels.

- A series of experiments demonstrate the superiority of the proposed method. Experimental results show that the Cross-CBAM network achieves a good trade-off between segmentation accuracy and inference speed. Specifically, Cross-CBAM-L1 network achieves 75.1% mIoU on the Cityscapes test set at a speed of 187.9FPS. Cross-CBAM-L2 achieves 77.2% mIoU and 88.6FPS under the same experimental setting.

2. Related work

2.1. Semantic Segmentation

Traditional semantic segmentation algorithms assign labels to each pixel using handcrafted features. With the development of deep convolutional neural networks, semantic segmentation has achieved outstanding performance. FCN[26] is the first full convolutional network for semantic segmentation. Due to its fully convolutional nature, it can segment any input image resolution. Furthermore, it is trained in an end-to-end and pixel-to-pixel manner. SegNet[1] proposed that the decoder perform non-linear upsampling using max-pooled indices. DeepLabv3[3] adopted a cascade or parallel ASPP module to capture multi-scale context by using multiple atrous rates. PSPNet[43] exploits the global contextual information with contextual aggregation based on different regions. However, most of these methods require substantial computational cost due to the high resolution of images. In this paper, we propose an efficient and effective segmentation model that achieves a good trade-off between speed and accuracy.

2.2. Real-Time Semantic Segmentation

Due to the limitation of computing resources, traditional semantic segmentation methods are greatly challenged. Therefore, lightweight semantic segmentation models are urgently needed to solve practical application problems. There are two mainstream approaches to designing efficient models. (1)*lightweight backbone*. MobileNet series[15, 31, 14] replaces traditional convolutions with depthwise separable convolutions. The depthwise separable convolution

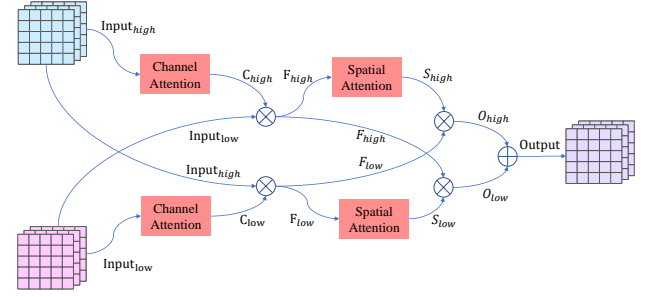


Figure 3: Diagram of CCBAM. We multiply the feature response from low-level with the feature from high-level, and multiply the feature response from high-level with the feature from low-level. Then, we add the obtained features to get the final output.

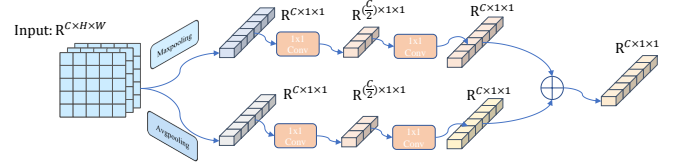


Figure 4: Diagram of Channel Attention Module.

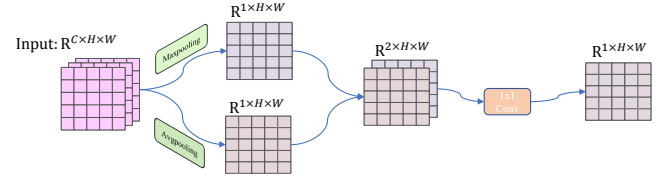


Figure 5: Diagram of Spatial Attention Module.

is composed of two parts: depthwise (DW) and pointwise (PW), and its number of parameters and operation cost are lower than traditional convolution. ShuffleNet[40] utilizes Pointwise Group Convolution and channel shuffle to reduce network capacity. (2)*lightweight decoder*. LEDNet[33] designs an attention pyramid network (APN) in the decoder to alleviate the complexity of the network. PP-LiteSeg[29] proposes a flexible and lightweight decoder (FLD), which reduces the computational load of the decoder.

2.3. Attention mechanism

Attention can be interpreted as a means of selectively focusing on a portion of all information. Squeeze-and-Excitation Network[17](SENet) uses global average pooling features to calculate channel-wise attention. It reweights feature channels to recalibrate channel-wise feature responses. Gather-Excite: Exploiting Feature Context in Convolutional Neural Networks [16](GENet) introduces a pair of operators: gather and excite. 'Gather' aggregates feature responses that are from a large spatial extent efficiently, and 'excite' redistributes the pooled information to local features. Convolutional Block Attention Module[34](CBAM) uses both

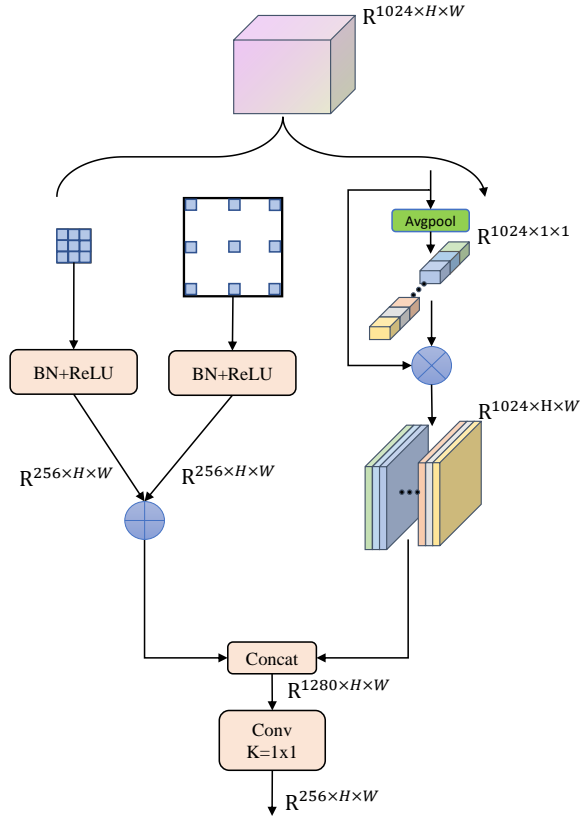


Figure 6: Details of the proposed SE-ASPP module. We adopt atrous convolution with dilation-rates=(1, 3), at the same time, the dilation rates can be adjusted dynamically.

channel attention and spatial attention to infer attention maps. The attention maps are then multiplied by the input feature map for feature refinement.

3. Proposed Method

In this section, we first introduce the Short-Term Dense Concatenate Module(STDC). Then Cross Convolutional Block Attention Module(CCBAM) and Squeeze-and-Excitation Atrous Spatial Pyramid Pooling Module(SE-ASPP) are recommended respectively. Finally, we show the whole structure of our real-time semantic segmentation model.

3.1. Short-Term Dense Concatenate Module

Typically, an encoder is designed to extract hierarchical features, the encoder consists of a series of layers grouped into several stages. As the number of convolutional neural network layers increases from shallow to deep, the number of channels gradually increases, and the spatial resolution gradually decreases. The Short-Term Dense Concatenate network[10] also has the same structure. Due to a large number of parameters, STDC abandoned the dual-stream path proposed by Bisenet[39] and switched to a single-path decoder. Due to the Short-Term Dense Concatenate structure and the design of Detail Guidance, it achieves 71.9% mIoU and 250.4FPS on the Cityscapes test set, which

is an excellent trade-off between accuracy and speed. Figure 2 illustrates the layout of the STDC module. Specifically, the STDC module is divided into several blocks, and each block includes one convolutional layer, one BN layer and a ReLU activation layer. The first block in the STDC module has a kernel size of 1, and the remaining blocks have a kernel size of 3. Assuming that the number of output channels of the STDC module are N , the number of output channels of the i -th block is $\frac{N}{2^i}$, except for the number of channels of the last block. It has the same number of output channels as the previous block. To enrich feature information, the STDC module concatenates the output feature maps of each block as the output of the STDC module through a skip path. Before concatenation, the feature maps from different blocks in the STDC module are down-sampled to the same spatial resolution by average-pooling operation with a pool size of 3×3 . The final output of the STDC module is:

$$x_{\text{output}} = F(x_1, x_2, \dots, x_n) \quad (1)$$

where x_{output} denotes the output of the STDC module, F denotes concatenate operation, and x_1, x_2, \dots, x_n denote the feature maps from all blocks.

3.2. Cross Convolutional Block Attention Module

Feature fusion plays a critical role in feature representation. Commonly used feature representation methods are element-wise summation and concatenation. But in this paper, we propose a new attention-based feature fusion module called CCBAM, which utilizes both channel attention and spatial attention. Different from the previous position of attention, CCBAM uses cross attention in the feature fusion of Encoder and decoder.

CCBAM Framework. As shown in figure 3, CCBAM has two input feature maps, and after passing through the channel attention module and the spatial attention module, the two inputs are fused into one output. In detail, the two input feature maps are denoted as $Input_{\text{high}}$ and $Input_{\text{low}}$. $Input_{\text{high}}$ is the output feature map of the decoder, and $Input_{\text{low}}$ is the counterpart of the decoder. $Input_{\text{high}}$ and $Input_{\text{low}}$ go through the channel attention module and generate channel-wise feature responses C_{high} and C_{low} , respectively. Then, We multiply $Input_{\text{low}}$ and C_{high} to get F_{high} , multiply $Input_{\text{high}}$ and C_{low} to get F_{low} . F_{high} and F_{low} go through the spatial attention module and generate spatial-wise feature responses S_{high} and S_{low} , respectively. After that, we multiply F_{low} and S_{high} to get the O_{high} , and multiply F_{high} and S_{low} to get the O_{low} . Finally, we apply element-wise operation to add O_{high} and O_{low} to get $Output$. Note that O_{high} and O_{low} have the same channels. As shown above, the designed module is called CCBAM since we cross-multiply feature maps and feature responses. We

formulate the above procedure as equation 2.

$$\begin{aligned}
C_{high} &= \text{Channel Attention}(Input_{high}) \\
C_{low} &= \text{Channel Attention}(Input_{low}) \\
F_{high} &= Input_{low} \cdot C_{high} \\
F_{low} &= Input_{high} \cdot C_{low} \\
S_{high} &= \text{Spatial Attention}(F_{high}) \\
S_{low} &= \text{Spatial Attention}(F_{low}) \\
Output &= ((F_{low} \cdot S_{high}) + (F_{high} \cdot S_{low}))
\end{aligned} \quad (2)$$

Channel Attention Module. In the channel attention module, both average pooling and max pooling operations are used to aggregate spatial information of a feature map. As shown in Figure 4, the size of the feature map for a given input is $R^{C \times H \times W}$. After max-pooling and average-pooling operations, two feature outputs will be generated, namely average-pooled feature and max-pooled features, and the dimension of each feature is $R^{C \times 1 \times 1}$. Then, convolution is performed with one hidden layer operation, and the hidden layer activation size is set to $R^{\frac{C}{r} \times 1 \times 1}$, where r is the reduction ratio ($r=16$ in our method). Finally, we combine the output feature maps with an element-wise summation. The procedure can be formulated as equation 3.

$$\begin{aligned}
C &= \text{Conv}(\text{Maxpooling}(Input)) + \\
&\quad \text{Conv}(\text{Avgpooling}(Input))
\end{aligned} \quad (3)$$

Spatial Attention Module. Different from channel attention, which focuses on 'what', spatial attention focuses on 'where'. As shown in Figure 5, given the input features $I^{C \times H \times W}$, first apply max pooling and average pooling along the channel axis to generate two 2D feature response maps, of which the dimension is $R^{1 \times H \times W}$. A concatenation operation is then applied to the two feature response maps and produces an effective feature descriptor, the dimension is $R^{2 \times H \times W}$. Afterwards, convolution and sigmoid operations are applied to generate a spatial attention map of dimension $R^{1 \times H \times W}$. Note that in CBAM, the kernel size of the last convolution operation is 7×7 , but only a 1×1 kernel is used for channel transformation in this work. The procedure can be formulated as equation 4.

$$\begin{aligned}
S &= \text{Conv}(\text{Concatenate}(\text{Maxpooling}(Input), \\
&\quad \text{Avgpooling}(Input)))
\end{aligned} \quad (4)$$

3.3. Squeeze-and-Excitation Atrous Spatial Pyramid Pooling Module

Atrous Spatial Pyramid Pooling Module has been proven to be effective in semantic segmentation tasks[3]. The atrous rates adopted by the ASPP module are 1, 12, 24, 36, which is of great help to effectively capture multi-scale information. However, large atrous rates, four parallel atrous convolutions and bilinear interpolation bring a huge amount of parameters and computational costs, which are not suitable for real-time semantic segmentation networks. Therefore, we design

Table 1

Details of the STDC networks. *ConvX* stands Conv-BN-ReLU. *KSize* means kernel size. *S*, *R*, *C* denote stride, the number of repetitions, and output channels respectively.

Stages	Output size	KSize	S	STDC1		STDC2	
				R	C	R	C
Image	224×224				3		3
ConvX1	112×112	3×3	2	1	32	1	32
ConvX2	56×56	3×3	2	1	64	1	64
Stage3	28×28		2	1	256	1	256
	28×28		1	1		3	
Stage4	14×14		2	1	512	1	512
	14×14		1	1		4	
Stage5	7×7		2	1	1024	1	1024
	7×7		1	1		2	

a Squeeze-and-Excitation Atrous Spatial Pyramid Pooling Module(SE-ASPP module), which has fewer parameters and faster inference speed for real-time. As shown in Figure 6. SE-ASPP consists of two parallel atrous convolutions and a SE attention module, one of which is 1×1 convolution with *rate* = 1, and the other is 3×3 convolution with *rate* = 3(All atrous convolution with 256 filters and batch normalization, and experiments show that 256 channels achieved trade-off between accuracy and speed). In addition, the bilinear interpolation upsampling in the ASPP module is computationally expensive, so the bilinear interpolation is discarded and the SE attention module is utilized. The resulting features from atrous convolution are added and then concatenate the resulting features from SE module. Finally, a convolutional layer is adopted for channel transformation.

3.4. Network Architecture

The proposed network structure is demonstrated in Figure 1. In the decoder, the STDC network[10] is chosen to extract hierarchical information. It has 5 stages, each of which downsamples the input with a stride of 2 to twice resolution, so that the final output feature map is only 1/32 of the size of the original image. Table 1 shows the details of the STDC network, only the output of stages 3,4,5 are used for feature fusion. This work proposes two versions of the network: Cross-CBAM-M and Cross-CBAM-L, where the decoders are STDC1[10] and STDC2[10] respectively. Cross-CBAM-M achieves faster inference speed, while Cross-CBAM-L achieves higher segmentation accuracy. First, we pass the output of the last layer of the encoder, that is, the output of stage 5, through the SE-ASPP module. A feature map is received, which has 256 channels and is 1/32 the size of the original image. Afterwards, an upsampling operation is applied to resize these feature maps to the size of the stage 4 output feature maps. Then, the CCBAM module is utilized to fuse the output from stage 4 and the resized feature maps. Next, we resize the output feature maps of Cross-CBAM to the size of the stage 3 output feature map. Finally, the CCBAM module is used to fuse the output feature maps of stage 3 and the resized feature maps.

Table 2

The comparisons with other state-of-the-art methods on Cityscapes. *no* means the method has no backbone. " - " indicates that the method does not give official data in their paper.

Model	Backbone	Resolution	mIoU(%) val test	FPS
ENet[28]	no	512x1024	-	58.3 76.9
LDFNet[19]	no	512x1024	68.4	71.3 27.7
BlseNetV2-L[38]	no	512x1024	75.8	75.3 47.3
CAS[41]	no	768x1536	-	70.5 108.0
GAS[22]	no	769x1537	-	71.8 108.4
HMSeg[20]	no	768x1536	-	74.3 83.2
FasterSeg[4]	no	1024x2048	73.1	71.5 163.9
MFNet[12]	no	512x1024	-	72.1 116
LSPANet[36]	no	1024x2048	-	77.1 60.3
SegFormer[37]	no	1024x1024	-	76.2 15.2
SETR-PUP[44]	no	768x768	-	78.4 -
EDANet[25]	EDANet	512x1024	-	67.3 108.7
ESPNetV2[27]	ESPV2	512x1024	66.4	66.2 -
LiteSeg[8]	ShuffleNet	512x1024	67.8	- 133.0
SFNet[21]	DF1	1024x2048	-	74.5 121.0
ICNet[42]	PSPNet50	1024x2048	-	69.5 30.3
MobilenetV3-L[14]	MobilenetV3	1024x2048	72.6	72.6 -
SegNext-T[14]	MSCAN-T	768x1536	-	78.0 25.0
STDC1-Seg50[10]	STDC1	512x1024	72.2	71.9 250.4
STDC2-Seg50[10]	STDC2	512x1024	74.2	73.4 188.6
STDC1-Seg75[10]	STDC1	768x1536	74.5	75.3 126.7
STDC2-Seg75[10]	STDC2	768x1536	77.0	76.8 97.0
PP-LiteSeg-T1[29]	STDC1	512x1024	73.1	72 273.6
PP-LiteSeg-B1[29]	STDC2	512x1024	75.3	73.9 195.3
PP-LiteSeg-T2[29]	STDC1	768x1536	76.0	74.9 143.6
PP-LiteSeg-B2[29]	STDC2	768x1536	78.2	77.5 102.6
Cross-CBAM-M1	STDC1	512x1024	74.19	73.4 240.9
Cross-CBAM-L1	STDC2	512x1024	76.04	75.1 187.9
Cross-CBAM-M2	STDC1	768x1536	76.14	75.5 119.7
Cross-CBAM-L2	STDC2	768x1536	78.35	77.2 88.6

In addition, due to the long tail problem of various data, an additional focal loss is adopted [23] to alleviate this problem. Focal loss was originally designed to address the one-stage object detection scenario and class imbalance. It originates from the cross entropy loss for binary classification, equation 5.

$$CE(p, y) = \begin{cases} -\log(p) & \text{if } y = 1 \\ -\log(1 - p) & \text{otherwise} \end{cases} \quad (5)$$

where $y \in \{\pm 1\}$ specifies the ground-truth class and $p \in [0, 1]$ is the model's estimated probability for the class with label $y = 1$. For convenience, it rewrites $CE(p, y) = CE(P_t) = -\log(p_t)$, $p_t = p$ if $y = 1$, else $p_t = 1 - p$. Focal loss adds a modulation factor $(1 - p_t)^\gamma$ to cross entropy loss, so as to remodel the loss function, reduce the weight of large scale targets, and focus on small targets training. It can be defined as:

$$FL(p_t) = -(1 - p_t)^\gamma \log(p_t) \quad (6)$$

Table 3

The comparisons with other state-of-the-art methods on CamVid. *no* means the method has no backbone. " - " indicates that the method does not give official data in their paper.

Model	Backbone	mIoU(%)	FPS
ENet[28]	no	51.3	61.2
CAS[41]	no	71.2	169
GAS[22]	no	72.8	153.1
EDANet[25]	no	66.4	-
BiseNetV2-L[38]	no	73.2	32.7
LSPANet[36]	no	73.0	73.5
MFNet[12]	no	71.5	145
DDRNet[13]	ResNet	74.7	230
BiseNetV1-L[39]	ResNet18	68.7	116.3
ICNet[42]	PSPNet50	67.1	34.5
TD4-PSP18[18]	PSPNet-18	72.6	40
STDC1-Seg[10]	STDC1	73.0	197.6
STDC2-Seg[10]	STDC2	73.9	152.2
PP-LiteSeg-T[29]	STDC1	73.3	222.3
PP-LiteSeg-B[29]	STDC2	75.0	154.8
Cross-CBAM-M	STDC1	73.8	185.3
Cross-CBAM-L	STDC2	75.6	146.8

Table 4

Ablation experiments of our proposed model on the Cityscapes validation set.

Model	SE-ASPP	Cross-CBAM	Aux-loss	mIoU(%)
Baseline				52.26
Cross-CBAM-M1 ✓				68.74
Cross-CBAM-M1		✓		72.63
Cross-CBAM-M1 ✓		✓		74.02
Cross-CBAM-M1 ✓		✓	✓	74.19

where $\gamma \in [0, 5]$ is a tunable parameter.

At the same time, with the increasing depth of the network, the parameters in the network are difficult to optimize, and the auxiliary loss can help optimize the learning process. In order to balance the main loss and auxiliary loss, a weight α is set to choose the proportion of main loss and auxiliary loss. The loss function in this paper is designed as: $Loss = \alpha CE + (1 - \alpha) FL$. Note that the auxiliary loss is only used during training, and during the testing phase, the auxiliary loss is abandoned and only the main branch is used.

4. Experiments Results

In this section, we first introduce the datasets used in this paper and the implementation details. Then, we compare the experimental results with existing models in terms of accuracy and inference speed. Finally, extensive ablation experiments are conducted to demonstrate the effectiveness of the proposed module.

Table 5

Atrous Rates Ablation Study. As can be seen from the table, dilation=(1,3) achieves a trade-off between speed and accuracy. Note that we set the number of channels of SE-ASPP to 256 and the input size to 512×1024 .

Dilations	mIoU	FPS	Flops(G)	Parameters(M)
(1,3)	74.19	241.1	11.31	12.21
(2,4)	74.20	229.5	12.39	14.31
(3,5)	75.30	229.4	12.39	14.31
(1,3,5)	74.61	226.4	12.52	14.57
(2,4,6)	74.15	225.1	13.60	16.67

Table 6

Comparisons with different channels on Cityscapes. Note that we set the atrous rates to (1,3). The Input size is set to 512×1024 .

Channels	mIoU	FPS	Flops(G)	Parameters(M)
512	73.86	235.7	14.77	19.54
256	74.19	240.9	11.31	12.21
128	72.21	245.6	9.67	8.92

4.1. Benchmarks and Evaluation Metrics

Cityscapes. The Cityscapes[7] is taken from the perspective of cars and is one of the well-known datasets focusing on the parsing of urban streetscape. It contains multiple stereoscopic video sequences recorded in street scenes from 50 different cities, with 5000 high-quality pixel-level annotations in addition to 20000 coarsely annotated frames. We only used 5,000 fine annotated images, 2,975 for training, 500 for validation, and 1525 for testing. Annotations include 30 classes, 19 of which are used for semantic segmentation tasks. Furthermore, the resolution of the image is as high as 1024×2048 , which is a great challenge for real-time semantic segmentation tasks.

CamVid. The CamVid[2] is taken from the perspective of a driving automobile, which is for road scene parsing. The database provides ground truth labels associating each pixel with one of 32 semantic classes, a subset of 11 classes are used for semantic segmentation experiment. The dataset contains 701 images with high-quality annotations, of which 367 images are used for training, 101 images for validation and 233 images for testing. The resolution of these images are 960×720 .

Evaluation Metrics. For accuracy evaluation, Mean of class-wise Intersection over Union(mIoU) is adopted as the evaluation metric. For speed evaluation, Frames Per Second(FPS) is adopted as the metric.

4.2. Implementation Details

Training Settings. As with most experiments, we choose mini-batch stochastic gradient descent(SGD) with a momentum of 0.9 and weight decay of $1 \times 5e^{-4}$ as the optimizer. The batch sizes of the Cityscapes and CamVid datasets are set to

16 and 24, respectively. Following the common configuration, 'poly' learning rate policy is adopted, where the initial rate is multiplied by $(1 - \frac{iter}{max_iter})^{power}$. We set the power as 0.9, the initial learning rate as 0.01 and the minimum learning rate as $1 \times e^{-4}$. We utilize the Cityscapes dataset to train the model for 160,000 iterations, utilize CamVid dataset to train the model for 10000 iterations. For data augmentation, random-crop, random-resize, and random-flip are included. For training Cityscapes, the cropped resolution is 512×1024 and the scale ranges in $[0.125, 0.5]$. For training CamVid, the cropped resolution is 960×720 and the scale ranges in $[0.5, 2.5]$. We conduct all experiments based on Pytorch-1.11, CUDA-11.3, CUDNN-8.4.1 environments. And all experiments are performed using MMsegmentation[6] on two GTX-1080Ti GPUs.

Inference Settings. In the inference phase, we export Cross-CBAM to ONNX format and utilize TensorRT for model inference. For Cityscapes, the resolution of the input images are 512×1024 and 768×1536 . For CamVid, the resolution of the input images are 960×720 . All inference experiments are conducted on a single NVIDIA GTX1080Ti GPU with batch size of 1 under CUDA-11.3, CUDNN-8.2.2.1, TensorRT-8.2.3.0.

4.3. Compare with State-of-the-arts

In this section, we conduct experiments on the Cityscapes dataset and the CamVid dataset to demonstrate that the proposed model achieves superior results. Then, the algorithm is compared with other existing state-of-the-art algorithms on two benchmarks, Cityscapes and CamVid.

Results on Cityscapes. As listed in Table 2, model name, input image resolution, backbone, mIoU and FPS of previous approaches are provided. Cross-CBAM-L1, Cross-CBAM-L2, respectively represent the input image resolution is 512×1024 , 768×1536 . Experimental results show that Cross-CBAM network achieve higher mIoU with excellent inference speed. Specifically, Cross-CBAM-M1 achieves 74.18% mIoU and 240.9 FPS on the validation set, about two percentage points higher than the STDC network[10], while retaining a competitive inference speed. Cross-CBAM-L1 achieves 76.04% mIoU and 187.9 FPS, which is a state-of-the-art trade-off between performance and speed. For a resolution of 768×1536 , Cross-CBAM-L2 achieves the highest accuracy-77.2% mIoU and 88.6FPS. Cross-CBAM-L2 achieves similar accuracy to LSPANet[36], but the inference speed of Cross-CBAM-L2 is 31.9% faster than LSPANet[36]. The Cross-CBAM series models achieves comparable accuracy to the PP-LiteSeg[29] series models while maintaining the superiority of inference speed. Furthermore, compared to SegNext[11], our model achieves 71.8% faster speed than SegNext at the expense of only 0.8% mIoU. Compared with SegFormer[37], although our model is slightly inferior to SegFormer[37] in accuracy, it has a great improvement in speed. We increase inference speed by 82.8%, from 25FPS to 88.6FPS. Therefore, it can be seen that the traditional convolution can also achieve results that

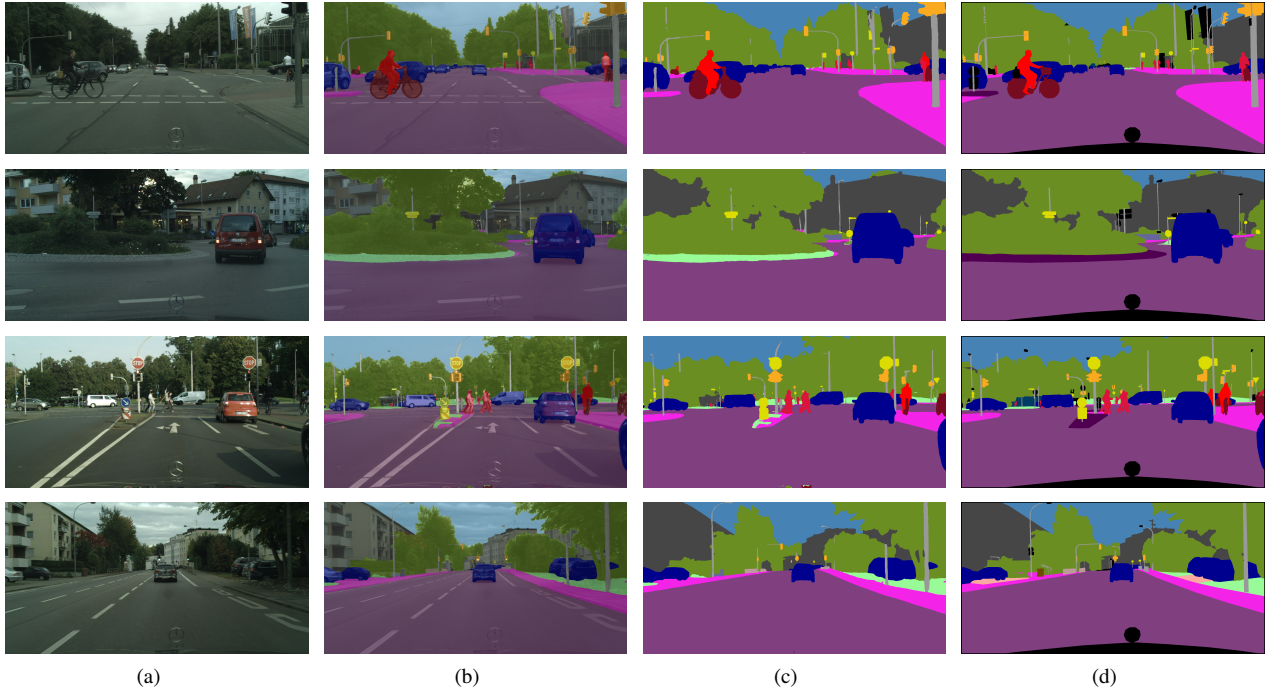


Figure 7: Visual segmentation results on Cityscapes validation set. The four columns from left to right represent the input image, the output of model(opacity=0.5), the output of model(opacity=1) and the ground truth.

are not inferior to the Transformer method, at least in the Cityscapes[7] dataset. Part of the segmentation results are shown in figure7.

Results on CamVid. To further verify the generalization of the model, we conduct experiments on the CamVid dataset. Following the previous methods, the input resolution for training and testing is set to 960×720 . As Table 3 shown, the model achieves 75.6% mIoU and 146.8 FPS, higher than the STDC2-Seg[10]. When compared to light-weight networks (ENet, CAS, GAS, EDANet), Cross-CBAM stands out among them on both speed and accuracy. Although STDC and PP-LiteSeg are faster than Cross-CBAM in terms of inference speed, Cross-CBAM achieves higher accuracy. Cross-CBAM-L is 2.6% mIoU higher than LSPANet[36] and 4.1% mIoU higher than MFNet[12], which is a considerable improvement for real-time semantic segmentation. At the same time, we have also made a huge breakthrough in inference speed, and our proposed method is 49.9% faster than LSPANet[36]. The comparison results demonstrate that Cross-CBAM has superior capability compared with other models.

4.4. Ablation Study

In this section, we conduct ablation experiments to validate the effectiveness of each component in Cross-CBAM. The Cross-CBAM-M1 model and the Cityscapes dataset are selected for the ablation study. Table 4 lists the results of the ablation experiments. The baseline model is STDC1 backbone+FCN segmentation head. The atrous rates of SE-ASPP in the ablation study are (1,3) and the number of channels

of SE-ASPP is 256. Adding the SE-ASPP module improves mIoU by 4.48%. The CCBAM module in Cross-CBAM-M1 improves the mIoU by 3.89%. Simultaneous use of SE-ASPP module and CCBAM module increases mIoU by another 1.39%. Meanwhile, adding an auxiliary segmentation head slightly improves segmentation accuracy. Figure 8 provides qualitative comparison results on the Cityscapes validation set. As modules are added one by one, the Cross-CBAM network can learn more detail information and becomes closer to the ground truth.

Atrous Rates Ablation Experiments As we all know, the more the number of atrous convolutions, larger the atrous rates, and the larger captured receptive fields. But more atrous convolutions and larger atrous rates are not suitable for real-time semantic segmentation. In order to balance accuracy and inference speed, we conduct ablation experiments with dilation rates (1,3), (2,4), (3,5), (1,3,5). Table 5 shows the results compared to different atrous rates. When the atrous rates are set to (1, 3), we achieve 74.19% mIoU, 241.1FPS, 11.31G Flops and 12.21M parameters at a resolution of 512×1024 . Atrous rates (3,5) achieve the highest mIoU, however, it corresponds to larger model, more parameters, and slower inference speed. Therefore, to balance accuracy and inference speed, the atrous rates of our model is set to (1,3).

Different SE-ASPP Channels In our intuitive impression, more channels in a neural network preserve more details, but in SE-ASPP module, the situation is different. As shown in Table 6, we initially set the channel of atrous convolution in

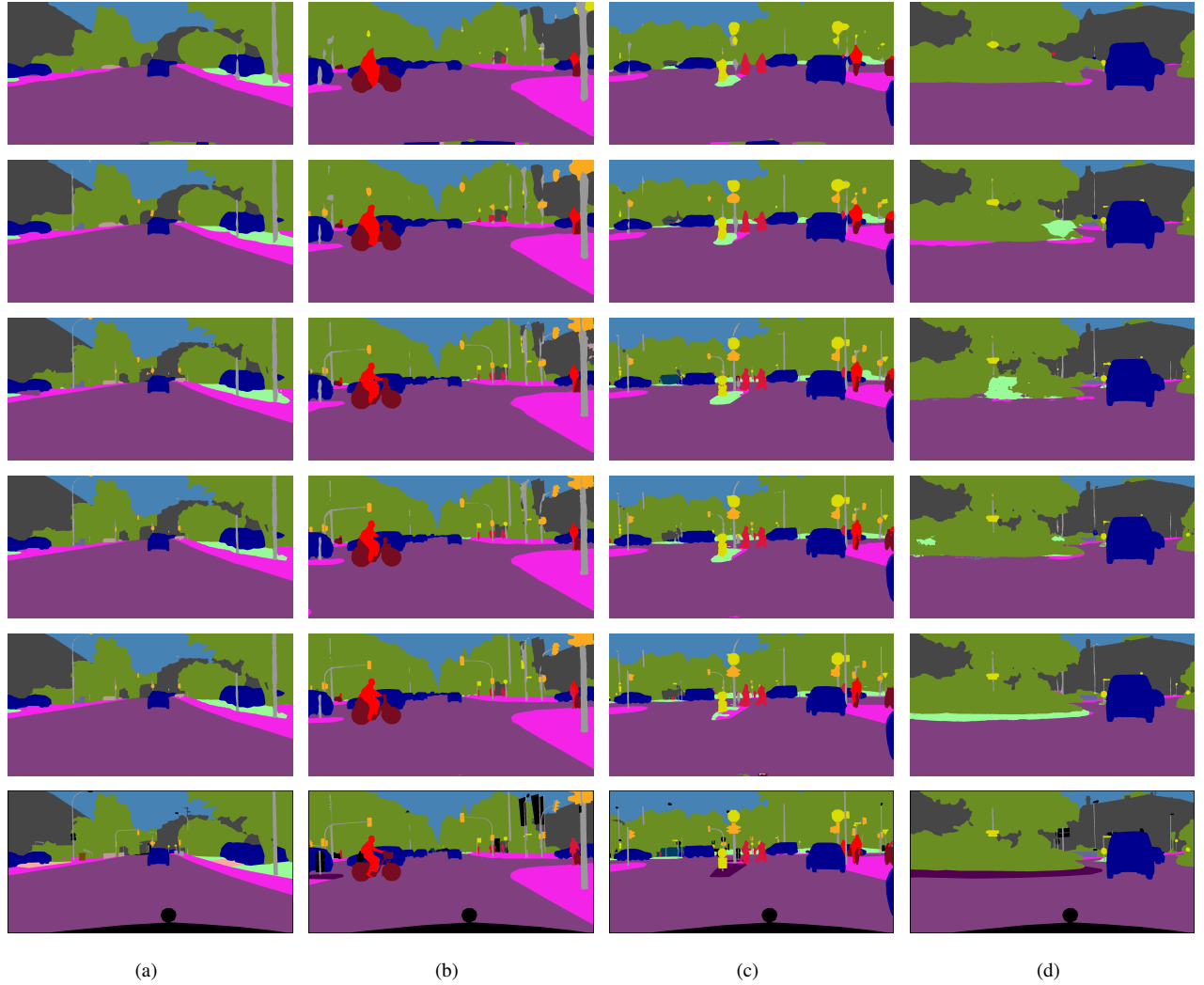


Figure 8: Visual qualitative comparison results on Cityscapes validation set. Six lines from top to bottom represent baseline, STDC1+SE-ASPP, STDC1+CCBAM, STDC1+SE-ASPP+CCBAM, STDC1+SE-ASPP+CCBAM+Aux-loss and ground truth in turn. We can observe that our proposed model can learn more small target information.

SE-ASPP to 512, resulting in a mIoU of 73.86%. However, when the channels are set to 512, we achieve 74.18% mIoU. Reducing the number of channels in SE-ASPP yields higher accuracy, meanwhile, reducing the number of channels also reduces the number of model parameters and improves inference speed. One possible reason is that more channels lead to redundancy and wrong combination of features. So when designing the model, we can change the way of thinking. It is not that the more channels the better.

5. Conclusions

In this paper, we choose the excellent STDC[10] network as the backbone of Cross-CBAM network. The STDC has a single path and adopts an aggregation of feature maps for image representation. We propose a new module for obtaining variable receptive fields at low computational cost, called Squeeze-and-Excitation Atrous Spatial Pyramid

Pooling Module(SE-ASPP). Meanwhile, it can obtain multi-scale information with fewer parameters and faster inference speed. Furthermore, to strengthen feature representation efficiently, we present a contextual attention fusion module named CCBAM, which leverages high-level semantic features to guide low-level detail features. And the low-level features are complementary to the high-level features. Based on these innovative modules, extensive experiments are conducted to demonstrate the effectiveness of the proposed modules. Meanwhile, our real-time semantic segmentation network achieves state-of-the-art trade-off between accuracy and inference speed.

CRedit authorship contribution statement

Zhengbin Zhang: Conceptualization of this study, Methodology, Software, Writing-original draft. **Zhenhao Xu:** Review & editing, Investigation, Project administration. **Xing-sheng Gu:** Supervision, Review & editing, Supervision. **Juan Xiong:** Hardware support, Review & editing.

Acknowledgement

This work is supported by the National Natural Science Foundation of China(61973120, 61673175, 61603139).

References

- [1] Badrinarayanan, V., Kendall, A., Cipolla, R., 2017. Segnet: A deep convolutional encoder-decoder architecture for image segmentation. *IEEE transactions on pattern analysis and machine intelligence* 39, 2481–2495.
- [2] Brostow, G.J., Fauqueur, J., Cipolla, R., 2009. Semantic object classes in video: A high-definition ground truth database. *Pattern Recognition Letters* 30, 88–97.
- [3] Chen, L.C., Papandreou, G., Schroff, F., Adam, H., 2017. Rethinking atrous convolution for semantic image segmentation. *arXiv preprint arXiv:1706.05587*.
- [4] Chen, W., Gong, X., Liu, X., Zhang, Q., Li, Y., Wang, Z., 2019. Fasterseg: Searching for faster real-time semantic segmentation. *arXiv preprint arXiv:1912.10917*.
- [5] Chollet, F., 2017. Xception: Deep learning with depthwise separable convolutions, in: *Proceedings of the IEEE conference on computer vision and pattern recognition*, pp. 1251–1258.
- [6] Contributors, M., 2020. MMSegmentation: Openmmlab semantic segmentation toolbox and benchmark. <https://github.com/open-mmlab/mms Segmentation>.
- [7] Cordts, M., Omran, M., Ramos, S., Rehfeld, T., Enzweiler, M., Benenson, R., Franke, U., Roth, S., Schiele, B., 2016. The cityscapes dataset for semantic urban scene understanding, in: *Proceedings of the IEEE conference on computer vision and pattern recognition*, pp. 3213–3223.
- [8] Emara, T., Abd El Munim, H.E., Abbas, H.M., 2019. Liteseg: A novel lightweight convnet for semantic segmentation, in: *2019 Digital Image Computing: Techniques and Applications (DICTA)*, IEEE. pp. 1–7.
- [9] Everingham, M., Van Gool, L., Williams, C.K., Winn, J., Zisserman, A., 2010. The pascal visual object classes (voc) challenge. *International journal of computer vision* 88, 303–338.
- [10] Fan, M., Lai, S., Huang, J., Wei, X., Chai, Z., Luo, J., Wei, X., 2021. Rethinking bisenet for real-time semantic segmentation, in: *Proceedings of the IEEE/CVF conference on computer vision and pattern recognition*, pp. 9716–9725.
- [11] Guo, M.H., Lu, C.Z., Hou, Q., Liu, Z., Cheng, M.M., Hu, S.M., 2022. Segnext: Rethinking convolutional attention design for semantic segmentation. *arXiv preprint arXiv:2209.08575*.
- [12] Ha, Q., Watanabe, K., Karasawa, T., Ushiku, Y., Harada, T., 2017. Mfnet: Towards real-time semantic segmentation for autonomous vehicles with multi-spectral scenes, in: *2017 IEEE/RSJ International Conference on Intelligent Robots and Systems (IROS)*, IEEE. pp. 5108–5115.
- [13] Hong, Y., Pan, H., Sun, W., Jia, Y., 2021. Deep dual-resolution networks for real-time and accurate semantic segmentation of road scenes. *arXiv preprint arXiv:2101.06085*.
- [14] Howard, A., Sandler, M., Chu, G., Chen, L.C., Chen, B., Tan, M., Wang, W., Zhu, Y., Pang, R., Vasudevan, V., et al., 2019. Searching for mobilenetv3, in: *Proceedings of the IEEE/CVF international conference on computer vision*, pp. 1314–1324.
- [15] Howard, A.G., Zhu, M., Chen, B., Kalenichenko, D., Wang, W., Weyand, T., Andreetto, M., Adam, H., 2017. Mobilenets: Efficient convolutional neural networks for mobile vision applications. *arXiv preprint arXiv:1704.04861*.
- [16] Hu, J., Shen, L., Albanie, S., Sun, G., Vedaldi, A., 2018a. Gather-excite: Exploiting feature context in convolutional neural networks. *Advances in neural information processing systems* 31.
- [17] Hu, J., Shen, L., Sun, G., 2018b. Squeeze-and-excitation networks, in: *Proceedings of the IEEE conference on computer vision and pattern recognition*, pp. 7132–7141.
- [18] Hu, P., Caba, F., Wang, O., Lin, Z., Sclaroff, S., Perazzi, F., 2020. Temporally distributed networks for fast video semantic segmentation, in: *Proceedings of the IEEE/CVF Conference on Computer Vision and Pattern Recognition*, pp. 8818–8827.
- [19] Hung, S.W., Lo, S.Y., Hang, H.M., 2019. Incorporating luminance, depth and color information by a fusion-based network for semantic segmentation, in: *2019 IEEE International Conference on Image Processing (ICIP)*, IEEE. pp. 2374–2378.
- [20] Li, P., Dong, X., Yu, X., Yang, Y., 2020a. When humans meet machines: Towards efficient segmentation networks, in: *The 31st British Machine Vision Virtual Conference*.
- [21] Li, X., You, A., Zhu, Z., Zhao, H., Yang, M., Yang, K., Tan, S., Tong, Y., 2020b. Semantic flow for fast and accurate scene parsing, in: *European Conference on Computer Vision*, Springer. pp. 775–793.
- [22] Lin, P., Sun, P., Cheng, G., Xie, S., Li, X., Shi, J., 2020. Graph-guided architecture search for real-time semantic segmentation, in: *Proceedings of the IEEE/CVF Conference on Computer Vision and Pattern Recognition*, pp. 4203–4212.
- [23] Lin, T.Y., Goyal, P., Girshick, R., He, K., Dollár, P., 2017. Focal loss for dense object detection, in: *Proceedings of the IEEE international conference on computer vision*, pp. 2980–2988.
- [24] Lin, T.Y., Maire, M., Belongie, S., Hays, J., Perona, P., Ramanan, D., Dollár, P., Zitnick, C.L., 2014. Microsoft coco: Common objects in context, in: *European conference on computer vision*, Springer. pp. 740–755.
- [25] Lo, S.Y., Hang, H.M., Chan, S.W., Lin, J.J., 2019. Efficient dense modules of asymmetric convolution for real-time semantic segmentation, in: *Proceedings of the ACM Multimedia Asia*, pp. 1–6.
- [26] Long, J., Shelhamer, E., Darrell, T., 2015. Fully convolutional networks for semantic segmentation, in: *Proceedings of the IEEE conference on computer vision and pattern recognition*, pp. 3431–3440.
- [27] Mehta, S., Rastegari, M., Shapiro, L., Hajishirzi, H., 2019. Espnetv2: A light-weight, power efficient, and general purpose convolutional neural network, in: *Proceedings of the IEEE/CVF conference on computer vision and pattern recognition*, pp. 9190–9200.
- [28] Paszke, A., Chaurasia, A., Kim, S., Culurciello, E., 2016. Enet: A deep neural network architecture for real-time semantic segmentation. *arXiv preprint arXiv:1606.02147*.
- [29] Peng, J., Liu, Y., Tang, S., Hao, Y., Chu, L., Chen, G., Wu, Z., Chen, Z., Yu, Z., Du, Y., et al., 2022. Pp-liteseg: A superior real-time semantic segmentation model. *arXiv preprint arXiv:2204.02681*.
- [30] Ronneberger, O., Fischer, P., Brox, T., 2015. U-net: Convolutional networks for biomedical image segmentation, in: *International Conference on Medical image computing and computer-assisted intervention*, Springer. pp. 234–241.
- [31] Sandler, M., Howard, A., Zhu, M., Zhmoginov, A., Chen, L.C., 2018. Mobilenetv2: Inverted residuals and linear bottlenecks, in: *Proceedings of the IEEE conference on computer vision and pattern recognition*, pp. 4510–4520.
- [32] Song, Q., Mei, K., Huang, R., 2021. Attanet: Attention-augmented network for fast and accurate scene parsing, in: *Proceedings of the AAAI Conference on Artificial Intelligence*, pp. 2567–2575.
- [33] Wang, Y., Zhou, Q., Liu, J., Xiong, J., Gao, G., Wu, X., Latecki, L.J., 2019. Lednet: A lightweight encoder-decoder network for real-time semantic segmentation, in: *2019 IEEE International Conference on Image Processing (ICIP)*, IEEE. pp. 1860–1864.
- [34] Woo, S., Park, J., Lee, J.Y., Kweon, I.S., 2018. Cbam: Convolutional block attention module, in: *Proceedings of the European conference on computer vision (ECCV)*, pp. 3–19.

- [35] Wu, Z., Shen, C., Hengel, A.v.d., 2017. Real-time semantic image segmentation via spatial sparsity. *arXiv preprint arXiv:1712.00213*.
- [36] Xiao, C., Hao, X., Li, H., Li, Y., Zhang, W., 2022. Real-time semantic segmentation with local spatial pixel adjustment. *Image and Vision Computing* 123, 104470.
- [37] Xie, E., Wang, W., Yu, Z., Anandkumar, A., Alvarez, J.M., Luo, P., 2021. Segformer: Simple and efficient design for semantic segmentation with transformers. *Advances in Neural Information Processing Systems* 34, 12077–12090.
- [38] Yu, C., Gao, C., Wang, J., Yu, G., Shen, C., Sang, N., 2021. Bisenet v2: Bilateral network with guided aggregation for real-time semantic segmentation. *International Journal of Computer Vision* 129, 3051–3068.
- [39] Yu, C., Wang, J., Peng, C., Gao, C., Yu, G., Sang, N., 2018. Bisenet: Bilateral segmentation network for real-time semantic segmentation, in: *Proceedings of the European conference on computer vision (ECCV)*, pp. 325–341.
- [40] Zhang, X., Zhou, X., Lin, M., Sun, J., 2018. Shufflenet: An extremely efficient convolutional neural network for mobile devices, in: *Proceedings of the IEEE conference on computer vision and pattern recognition*, pp. 6848–6856.
- [41] Zhang, Y., Qiu, Z., Liu, J., Yao, T., Liu, D., Mei, T., 2019. Customizable architecture search for semantic segmentation, in: *Proceedings of the IEEE/CVF Conference on Computer Vision and Pattern Recognition*, pp. 11641–11650.
- [42] Zhao, H., Qi, X., Shen, X., Shi, J., Jia, J., 2018. Icnet for real-time semantic segmentation on high-resolution images, in: *Proceedings of the European conference on computer vision (ECCV)*, pp. 405–420.
- [43] Zhao, H., Shi, J., Qi, X., Wang, X., Jia, J., 2017. Pyramid scene parsing network, in: *Proceedings of the IEEE conference on computer vision and pattern recognition*, pp. 2881–2890.
- [44] Zheng, S., Lu, J., Zhao, H., Zhu, X., Luo, Z., Wang, Y., Fu, Y., Feng, J., Xiang, T., Torr, P.H., et al., 2021. Rethinking semantic segmentation from a sequence-to-sequence perspective with transformers, in: *Proceedings of the IEEE/CVF conference on computer vision and pattern recognition*, pp. 6881–6890.
- [45] Zhou, B., Zhao, H., Puig, X., Xiao, T., Fidler, S., Barriuso, A., Torralba, A., 2019. Semantic understanding of scenes through the ade20k dataset. *International Journal of Computer Vision* 127, 302–321.